Arctic Sea State 2015 Field Campaign, Version 1

USER GUIDE

How to Cite These Data

As a condition of using these data, you must include a citation:

Thomson, J. and O. Persson. 2021. *Arctic Sea State 2015 Field Campaign, Version 1*. [Indicate subset used]. Boulder, Colorado USA. NSIDC: National Snow and Ice Data Center. https://doi.org/10.7265/qt2b-y743. [Date Accessed].

FOR QUESTIONS ABOUT THESE DATA, CONTACT NSIDC@NSIDC.ORG

FOR CURRENT INFORMATION, VISIT https://nsidc.org/data/G10030

National Snow and Ice Data Center

TABLE OF CONTENTS

1 DATA DESCRIPTION

1.1 Summary

The U.S. Office of Naval Research (ONR) Sea State Departmental Research Initiative (DRI) field campaign was conducted during autumn of 2015 in the Beaufort Sea in order to better understand how waves and ice interact as Arctic ice advances in late autumn. Data collection took place under four sampling modes: wave experiments, ice stations, flux stations, and ship surveys. Data acquired during ice stations, flux stations, and ship surveys are provided in a single NetCDF ship data file. The timeseries in the file goes from 01 October 2015 through 07 November 2015, with a timestep of 10 minutes. Wave experiment data were acquired using six Surface Wave Instrument Float with Tracking (SWIFT) buoys and are in separate NetCDF files. The SWIFT buoy data are from 02 October 2015 through 02 November 2015 with a timestep of 30 minutes. Note that concurrent records from up to six drifters did sometimes occur during the campaign.

Figure 1. Arctic Sea State 2015 Logo

1.2 Background

In late September 2015, the Research Vessel (R/V) *Sikuliaq* departed Nome, AK and headed through the Bering Strait and into the Beaufort Sea north of Point Barrow. Over a six-week field campaign, measurements were taken outside of the ice edge, in the marginal ice zone, and within pack ice. During this time, the ice advanced irregularly toward the North Slope of Alaska (Figure 2). By November 1, sea ice met the coast east of Point Barrow, and the *Sikuliaq* headed south to Dutch Harbor, AK.

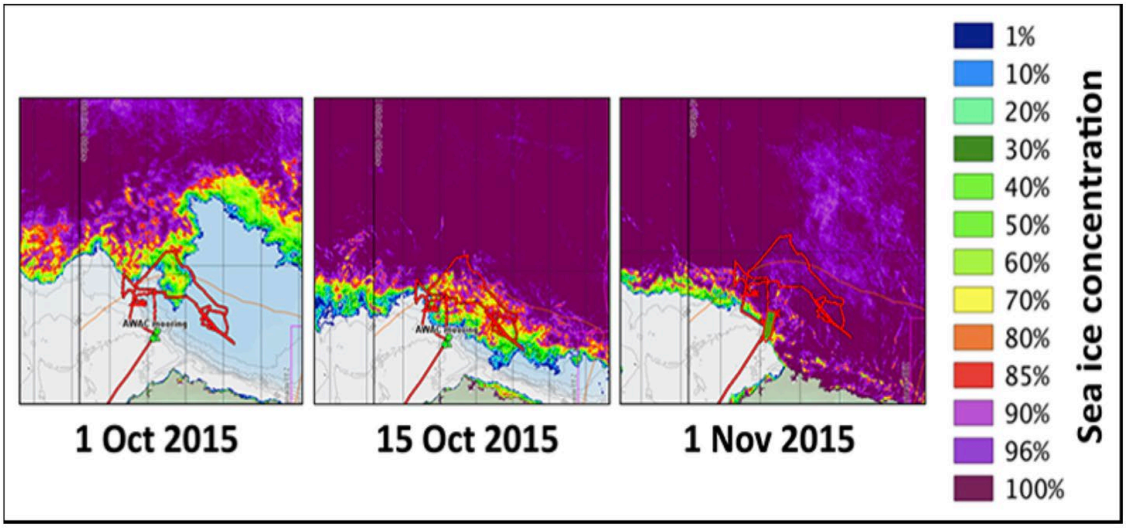

Figure 2. Ship track (red track), bathymetry (blue shading), and satellite-based ice concentrations (colors). These images were captured from the map server on board the R/V *Sikuliaq* as it displayed images from the University of Bremen showing ice concentration from passive microwave Advanced Microwave Scanning Radiometer 2 (AMSR2) data. Credit: Ola Persson (University of Colorado/ Cooperative Institute for Research in Environmental Sciences and NOAA Physical Science Laboratory).

The Sea State and Boundary Layer Physics of the Emerging Arctic Ocean program, sponsored by ONR, conducted the field campaign in order to better understand how waves and ice interact as Arctic ice advances in late autumn as well as to understand the seasonal evolution of sea ice and the effect of increasing open water on the ice and on the atmosphere. As sea ice has retreated under the influence of warming climate, fetch (distance of open water over which wind can act to build waves) has grown, resulting in an increasingly dynamic sea state. The melt season has gotten longer, giving ocean swell more time in which to build. Pancake ice, previously uncommon, is now characteristic of the western Arctic in autumn. The Sea State program worked to include wave-ice interactions in a wave forecast model, and then to refine the model with what was learned from the field program. The main goals of the Sea State program (as listed on the ONR Sea State web site) are the following:

- Develop a sea state climatology, identify factors affecting the spatial and temporal variability of sea state, and improve forecasting of waves on the open ocean and in the marginal ice zone.
- Develop a climatology of and improve theory of wave attenuation/scattering in the sea ice cover.
- Use wave scattering theory directly in integrated Arctic system models, and indirectly to define an ice rheology for use in Arctic system models.
- Understand the physics of heat and mass transfer from the ocean to the atmosphere, and the seasonal variability of fluxes during summer ice retreat and autumn ice advance.

When waves propagate into a marginal ice zone (area where Arctic sea ice meets the open ocean), the ice scatters and damps the waves with an effectiveness that depends on floe size and concentration. Waves, in turn, may break up ice or influence how it forms. Modeling the interaction is challenging. To meet the challenge, every aspect of energy exchange between air and sea that could be observed from the R/V *Sikuliaq* and from autonomous instruments around the ship was measured. The focus on the ice edge and just inside it where ice was forming meant that instrument systems had to be repositioned as the ice edge moved over the course of the field campaign.

Several articles describe the field experiment and provide contextual information that will be useful to users of these data. These articles are listed in the References section.

Under the sponsorship of ONR, NSIDC is serving as the long-term archive and distribution point for most Sea State in situ field experiment data. The data we hold may duplicate some of the data held in other archives. These archives are listed under the Related Websites section.

This data collection holds the following data:

- Ship data: Includes conductivity, temperature, and depth (CTD) casts and visual ice observations as well as data from shipboard instrumentation.
- SWIFT buoy data: Includes ocean surface salinity and temperature, ocean surface drift, surface winds, and atmospheric pressure and temperature at a 1 m height, in addition to peak wave period, peak wave direction, significant wave height, and wave energy spectral density as a function of frequency.

See the Related Websites section if you are in search of other Sea State data such as Acoustic Wave and Current (AWAC) mooring data or National Institute of Water and Atmospheric Research (NIWA) wave buoy data.

1.3 Parameters

1.3.1 Ship Data

The documentation describing ship data is drawn from Persson et al. (2018), hereafter JGR2018. JGR2018 describes the acquisition and processing of survey data from the four in-ice transits and flux station data from the four periods during which the ship was quasi-stationary near the ice edge. All of the parameters held as variables in ArcticSeaState2015_shipdata.nc are described in JGR2018 along with some that are not included in the NetCDF file. All of the parameters listed in the JGR2018 groupings below have values that are either measured directly or are arrived at using the variables held in the shipboard data file. The list below is included for completeness, but note

that not all parameters in the list below are included in the ArcticSeaState2015_shipdata.nc file. For example, tropospheric profiles are not included but are described in Guest et al. (2018). For a complete list of all the included shipboard data variables that are included in the NetCDF file, see Table 1 and Appendix A .

JGR2018 groups parameters as follows:

- Time and ship navigational information
- Directly Measured Meteorological and Air-Surface Flux Parameters [JGR2018 2.1, Table 1]
    - Air temperature, humidity, air pressure, wind speed and direction
    - Covariance and inertial dissipation calculations of turbulent sensible heat flux, latent heat flux, and momentum flux
    - Tropospheric profiles of pressure, temperature, humidity, and wind
    - Cloud base, cloud fraction from ceilometer
    - Downwelling shortwave and longwave broadband radiation
- Surface Parameters [JGR2018 2.2, Table 2]
    - Surface or skin temperature (measured by three techniques)
    - Near-surface upper ocean salinity
    - Ocean wave characteristics
    - Surface ice types and parameters (manual and sensor observation techniques)
- Upper-Ocean Parameters [JGR2018 2.3, Table 3]
    - Underway profiles of pressure, temperature, salinity
- Derived Parameters [JGR2018 2.4, Table 4)
    - Sea ice thickness, drift speed and direction
    - Surface albedo and emissivity
    - Net atmospheric energy flux
    - Atmosphere-surface bulk turbulent sensible heat, latent heat, and momentum fluxes
    - Atmospheric mixed layer height
    - Ocean mixed layer depth
    - Ocean freezing point
    - Ocean excess temperature

1.3.2 SWIFT Drifting Buoy Data

Documentation describing SWIFT drifter data is drawn from Thomson (2012), Smith et al. (2018), and Smith and Thomson (2019).

Parameters measured with SWIFT buoy data include the following:

- Wind speed and direction measured by Airmar PB200 ultrasonic anemometer
- Wave spectra, height, period, and direction derived from buoy motions measured by Microstrain 3DM-GX3-35 GPS and Inertial Motion Unit
- Temperature and salinity at 0.5 m depth measured by Aanderra Connectivity-Temperature Sensor
- Air pressure and temperature measured by Airmar PB200 meterological station

Table 4 lists and describes all included SWIFT data variables.

1.4 File Information

1.4.1 Format

There are 31 data files in this data set, all in NetCDF format. One file contains a time series of ship data and 30 files contain data from the six SWIFT buoys.

1.4.2 File Contents and Naming Convention

1.4.2.1 Ship Data

All of the ship surveys, ice station data, and flux station data reside in a single NetCDF file: ArcticSeaState2015_shipdata.nc. The sensors, sampling rates, and sensor locations of the instruments that provided these data are listed In JGR2018 Tables 1-3. Table 1 (in this document) lists the parameters held as variables in ArcticSeaState2015_shipdata.nc. Those descriptions repeat or paraphrase those in the NetCDF file. Appendix A has an extended version of Table 1 with more information about the variables and with references to JGR2018 tables for some variables. There is not a one-to-one relationship between the parameters listed in JGR2018 tables and the variables in the shipboard NetCDF file.

For the ship data, variable values are given every 10 minutes for 0October 2015 (day 274) through 07 November 2015 (day 311) along the R/V *Sikuliaq* track. Variables measured less frequently than every 10 minutes are assigned to the nearest 10-minute interval, with in-between intervals given a *missing* value of 9999. 10-minute averages (or interpolations for wave parameters) are used for some parameters.

Many of the data are from instruments belonging to the NOAA ESRL Physical Sciences Laboratory (PSL, formerly Physical Sciences Division (PSD)). However, some data stem from instruments belonging to the R/V *Sikuliaq*, the Naval Postgraduate School, University of Miami, University of Washington, and University of Texas-San Antonio.

Table 1. Description of variables in the ArcticSeaState2015_shipdata.nc file (alphabetical order). See Appendix A for an expanded version of this table.

Variable Name	Description
Ai	Best estimate of ice concentration in percent
alb_ref	Surface albedo estimated from the observed surface conditions (ice conc, snow depth, skin temperature, water freezing point) and subjective estimates of albedo: 0.08 = open water, 0.35 = thin ice, 0.65 = thicker ice, 0.85 = snow covered ice
cld_bas_ref	Median cloud base from ceilometer, m

Variable Name	Description
cld_frc_ref	Cloud fraction (%); percent of time within 10-min period that ceilometer detected a cloud
cog_ref	GPS course over ground (degrees)
ctd6m_frzT_ref	Freezing point at 6 m depth (deg C)
ctd6m_S_ref	CTD salinity at 6 m (PSU)
ctd6m_T_ref	CTD temperature at 6 m (deg C)
emiss_ref	Surface emissivity estimated from surface type/conditions: 0.99 = open water, 0.985 = ice covered water
fatm	Net atmospheric energy flux (W/m2) fatm = swd_bst_ref - swu + lwd_bst_ref - lwu - hs_blk_ref - hl_blk_ref
floe_size_ref	ASSIST floe size code for ice type with greatest concentration: 100 – pancakes 200 – new sheet ice 300 – Brash/broken ice 400 – cake ice (<20m) 500 – small floes (20-100m) 600 – medium floes (100-500m) 700 – large floes (500-2000m) 800 – vast floes (>2000m) 900 – bergy floes
hed_ref	GPS heading (degrees)
hl_blkr	Latent heat flux -bulk as for sensible heat flux (W/m2)
hlc_ref	Latent heat flux - covariance (W/m2)
hlid_ref	Latent heat flux - inertial dissipation (W/m2)
hs_blkr	Sensible heat flux - bulk calculated using COARE and SHEBA flux (W/m2) schemes depending on mosaic method & mean ice concentration. Neither scheme was developed for mixed waves and ice.
hsc_ref	Sensible heat flux -covariance (W/m2)
hsid_ref	Sensible heat flux - inertial dissipation (W/m2)
Hsig_Rgl_ref	Significant wave height from 1-D Riegl (m)
ice_concvo_ref	Total ice concentration from visual observations from 0-10 (tenths)
ice_typ1vo_ref	ASSIST primary ice type from visual observations: 10 - Frazil 11 - Shuga 12 - Grease 13 - Slush 20 - Nilas 30 - Pancakes 40 - Young Grey Ice, 10-15cm 50 - Young Grey Ice, 15-30cm 60 - First Year, < 70cm 70 - First Year, 70-120cm 75 - Second Year 80 - First Year, > 120cm 85 - Multiyear 90 - Brash
ice_z_ref	Ice thickness estimates from visual observations (cm)

Variable Name	Description
iceconcSEB_ref	10-min ice concentration from thermodynamic technique (%)
iconcsh_amsr_ref	Ice concentration from daily AMSR2 (3.125 km res) (%)
ieaz_ref	Azimuth to nearest ice edge (degrees)
iedis_ref	Distance to nearest ice edge (km)
ieor_ref	Orientation of nearest ice edge (deg)
jd_ref	Decimal day-of-year for 2015, values range from 274 (01 October 2015) to 311 (07 November 2015)
lat_ref	Latitude (degrees)
lon_ref	Longitude (degrees)
lwd_bst_ref	Downwelling LW radiation, gaps estimated from ceilometer and soundings (W/m2)
lwd_med_ref	Downwelling LW radiation, manually edited (W/m2)
lwu	Upwelling longwave radiation estimated from composite skin temperature, estimated surface emissivity, and Stefan-Boltzmann relation& mosaic method with ice concentration (W/m2)
mlh_ref	Atmospheric mixed-layer height at times of soundings (m)
omld_ref	Ocean mixed-layer depth from uCTDs (m)
omlheat_ref	Heat content of ocean mixed-layer (J/m2)
omlp15heat_ref	Heat content of ocean layer between OMLD and OMLD+15 m (J/m2)
omlxcsheat_ref	Excess heat content (above freezing point) of ocean mixed-layer (J/m2)
p_mb_ref	Atmospheric pressure at height zp (mb)
pcp_ref	Precipitation rate (set to 0.1 mm/h when logs indicated precipitation; otherwise 0)
qa_ref	Specific humidity (g/kg)
qs_ref	Surface saturation specific humidity (g/kg)
radar_icedrift_dir_ref	Marine radar ice drift direction (degrees clockwise from N)
radar_icedrift_spd_ref	Marine radar ice drift speed (m/s)
radar_sfccurr_dir_ref	Marine radar surface current direction (degrees clockwise from N)
radar_sfccurr_spd_ref	Marine radar surface current speed (m/s)
radar_wave_dp_ref	Marine radar peak wave direction (degrees clockwise from N)
radar_wave_tp_ref	Marine radar peak wave period (s)
rh_ref	Relative humidity (percent)
rwdir_ref	Relative wind direction, composite (+/- 180 deg from bow)
rwspd_ref	Relative wind speed, composite (m/s)
sal_ref	Salinity at ship intake at 6.5 m depth (PSU)

Variable Name	Description
slp_ref	Sea-level pressure by height-correcting p_mb_ref (mb)
snow_z_ref	Snow depth estimates from visual observations (cm)
sog_ref	GPS ship speed over ground (m/s)
std_hed_ref	Standard deviation in gyro heading (degrees)
std_rwdir_ref	Standard deviation rel wind direction, composite (degrees)
std_rwspd_ref	Standard deviation rel wind speed, composite (m/s)
std_sog_ref	Standard deviation in sog (m/s)
swd_bst_ref	Downwelling SW radiation, linear interpolation across gaps (W/m2)
swd_med_ref	Downwelling SW radiation, manually edited (W/m2)
swu	Upwelling shortwave radiation estimated from best downwelling SW radiation and estimated surface albedo & mosaic method with ice concentration (W/m2)
ta_ref	Air temperature (deg C)
tau_blkr	Bulk stress (N/m2), as for sensible heat flux
tauc_ref	Stress - covariance (N/m2)
tauid_ref	Stress - inertial dissipation (N/m2)
to_frz_ref	Freezing point of sea water from salinity from ship intake at 6.5 m depth (deg C)
Tpi_Rgl_ref	Max wave period from 1-D Riegl (s), doppler corrected in the manner of Collins et al. (2017)
ts_skn_ref	Composite skin temperature from ship-based IR sources (deg C)
ts_snk_ref	Sea-snake temperature when deployed at either 10 cm depth or on top of ice/snow (deg C)
wdir_ref	True wind direction, composite (degrees)
wspd_ref	True windspeed, composite (m/s)
zice_dpnt_ref	Ice thickness from dipnet (m)
ziceSEBmd_ref	10-min median of 1-s ice thickness from thermodynamic technique (m), mean of two KT-15 radiometers
zicesig_ref	10-min standard deviation of 1-s ice thickness values from TD technique (m)
zp_ref	Air pressure measurement height (m)
zq_ref	Air humidity measurement height (m)
zt_ref	Air temperature measurement height (m)
zu_ref	Wind speed measurement height, composite (m)

1.4.2.2 SWIFT Drifting Buoy Data

Over the course of the Sea State 2015 field campaign, a suite of six buoys were deployed in the same general location and then retrieved hours or days later before the ship moved on for another deployment of buoys. Seven of these surveys, called wave arrays, took place along with two other deployments during other times in the campaign for a total of nine deployments. The Sea State 2015 Cruise Report documents these deployments.

All individual buoy records are in separate SWIFT NetCDF files. SWIFT observations of surface winds, waves, temperature, and salinity occur in 8-minute bursts of raw data collected five times an hour and are postprocessed into 30-minute intervals for bulk statistical quantities (Smith et al., 2018). The data from buoys that are in the water at the same time will have identical time stamps.

These data are provided in 30 NetCDF files located in the `SWIFT-files` directory via HTTPS: https://noaadata.apps.nsidc.org/NOAA/G10030/ with the following naming convention and as described in Table 2.

SWIFTXX_[DD]-DDMMYYYY_30min.nc

Table 2. SWIFT buoy file naming convention

Variable	Description
SWIFTXX	Buoy number where XX is 09, 11, 12, 13, 14, or 15.
[DD]-DDMMYYYY	Day, month, and year of the data within the SWIFT file. The files may either contain a single day of data (DDMMYYY) or a range (DD-DDMMYYY).
30min	Indicates that the data are sampled at 30-minute intervals.
.nc	Identifies this as a NetCDF file.

The nine deployments are known as Wave Array 1 - 7, Ice Station 1, and Racetrack. The SWIFT buoy data files are organized into directories based on these survey names. Table 3 lists the buoys deployed in each of the nine surveys and their associated data files.

Table 3. SWIFT buoy data deployment names and data files

Deployment Name	Buoy Numbers	File Names
Wave Array 1	12	SWIFT12_02Oct2015_30min.nc
Wave Array 2	11,12,14	SWIFT11_04Oct2015_30min.nc SWIFT12_04Oct2015_30min.nc SWIFT14_04Oct2015_30min.nc

Deployment Name	Buoy Numbers	File Names
Wave Array 3	09, 11, 12, 13, 14, 15	SWIFT09_11-14Oct2015_30min.nc SWIFT11_10Oct2015_30min.nc SWIFT11_11-14Oct2015_30min.nc SWIFT12_11-14Oct2015_30min.nc SWIFT13_11-14Oct2015_30min.nc SWIFT14_10Oct2015_30min.nc SWIFT14_11-13Oct2015_30min.nc SWIFT15_11-13Oct2015_30min.nc
Wave Array 4	11, 12, 14, 15	SWIFT11_16-18Oct2015_30min.nc SWIFT12_16-17Oct2015_30min.nc SWIFT14_16-18Oct2015_30min.nc SWIFT15_16-18Oct2015_30min.nc
Wave Array 5	12	SWIFT12_18Oct2015_30min.nc
Wave Array 6	09, 11, 12, 13, 14, 15	SWIFT09_23-24Oct2015_30min.nc SWIFT11_23-24Oct2015_30min.nc SWIFT12_23-24Oct2015_30min.nc SWIFT13_23-24Oct2015_30min.nc SWIFT14_23-24Oct2015_30min.nc SWIFT15_23-25Oct2015_30min.nc
Wave Array 7	09, 11, 13, 15	SWIFT09_31Oct-01Nov2015_30min.nc SWIFT11_31Oct-01Nov2015_30min.nc SWIFT13_31Oct-01Nov2015_30min.nc SWIFT15_31Oct-01Nov2015_30min.nc
Ice Station 1	09, 12	SWIFT09_06-08Oct2015_30min.nc SWIFT12_06-08Oct2015_30min.nc
Racetrack	09	SWIFT09_02Nov2015_30min.nc

Table 4 describes the variables in the SWIFT buoy files. Variable descriptions in Table 4 repeat or paraphrase those in the NetCDF files with some additional information taken from information that was supplied to NSIDC along with the NetCDF files.

Table 4. Variables in all SWIFT buoy files (alphabetical order)

Variable Name	Description
a1	Normalized spectral directional moment (positive east) (m^2/Hz)
a2	Normalized spectral directional moment (east-west) (m^2/Hz)
airpres	Air pressure (atm)
airpresstddev	Standard deviation of air pressure (atm)
airtemp	Air temperature (deg C) at 1 m height above the wave-following surface (9999 for missing)

Variable Name	Description
airtempstddev	Standard deviation of air temperature (deg C)
b1	Normalized spectral directional moment (positive north) (m^2/Hz)
b2	Normalized spectral directional moment (north-south) (m^2/Hz)
check	Quality metric for the wave spectra (1 represents high quality results). See Eq 2 in Thomson et al. (2015)
driftdirT	Drift direction TOWARDS (degrees True) (equivalent to "course over ground")
driftdirTstddev	Standard deviation of direction of SWIFT drift (degrees)
driftspd	Speed of SWIFT drift (m/s) (equivalent to "speed over ground")
driftspdstddev	Standard deviation of speed of SWIFT drift (m/s)
energy	Wave energy spectral density (m^2/Hz) as a function of frequency. Note that this is derived from orbital motions and is thus insensitive to low-energy swell conditions. The technique is best suited to measuring short wind waves.
freq	Spectral frequencies (Hz)
lat_lagrangian	Latitude (decimal degrees North)
lon_lagrangian	Longitude (decimal degrees East)
peakwavedirT	Wave direction at energy peak (degrees from North) (9999 for missing)
peakwaveperiod	Wave period at peak of energy spectrum (s)
salinity	Water salinity (PSU) at 0.5 m below the surface
sigwaveheight	Significant wave height (m)
time	Days since 1970-01-01 00:00:00 UTC
watertemp	Water temperature (deg C) at 0.5 m below the surface
winddirT	True wind direction (degrees from North) (9999 for missing)
winddirTstddev	Standard deviation of true wind direction (degrees)
windspd	Wind speed (m/s) at 1 m height above the wave-following surface (9999 for missing)
windspdstddev	Standard deviation of wind speed (m/s)

1.5 Spatial Coverage

1.5.1 Ship Data

The following are the approximate latitude/longitude bounding coordinates of the ship data:

Northernmost Latitude: 75.476° N
Southernmost Latitude: 62.759° N
Easternmost Longitude: 148.532° W
Westernmost Longitude: 168.489° W

1.5.2 SWIFT Drifting Buoy Data

The following are the approximate latitude/longitude bounding coordinates of the SWIFT buoy data:

Northernmost Latitude: 75.451° N
Southernmost Latitude: 69.958° N
Easternmost Longitude: 148.565° W
Westernmost Longitude: 161.151° W

1.6 Temporal Information

1.6.1 Coverage

The shipboard data run from 01 October 2015 to 07 November 2015 and the SWIFT buoy data run from 02 Oct 2015 to 02 November 2015.

1.6.2 Resolution

1.6.2.1 Ship Data

The shipboard data NetCDF file has values every 10 minutes.

1.6.2.2 SWIFT Drifting Buoy Data

SWIFT observations of surface winds, waves, temperature, and salinity occur in 8-minute bursts of raw data collected five times an hour. These are postprocessed into half-hour intervals (Smith et al., 2018).

2 DATA ACQUISITION AND PROCESSING

2.1 Acquisition

2.1.1 Ship Data

JGR2018 describes the acquisition and processing of survey data from the four in-ice transits and flux station data from the four periods during which the ship was quasi-stationary near the ice edge. These data were acquired by a team led by Ola Persson. Persson and colleagues wrote code to process the raw data into a timeseries of observed and derived parameters listed in Table 1. NSIDC acquired the processed data as a NetCDF file from Sea State PI Thomson in April 2020. No processing took place at NSIDC.

2.1.2 SWIFT Drifting Buoy Data

Observations of surface winds, waves, temperature, and salinity occur in 8-minute bursts of raw data collected five times an hour. These are postprocessed into half-hour intervals for bulk statistical quantities (Smith et al., 2018). The time variable in the NetCDF file repeats because the single file holds data from several concurrent deployments.

Smith and Thomson 2019 and Smith et al. 2018 describe aspects of SWIFT data processing that were used with Sea State data. More fundamental aspects of SWIFT data are described in Thomson 2012. The code that produced the post-processed 30-minute interval data was written by Jim Thomson and ran at University of Washington. All SWIFT processing codes are publicly available on github: https://github.com/jthomson-apluw/SWIFT-codes.

NSIDC acquired the processed data as NetCDF files from Sea State PI Thomson in May 2021. No processing took place at NSIDC.

Figure 3 and Figure 4 illustrate aspects of the SWIFT data. These figures were made using the NASA Panoply NetCDF data viewer. In Figure 3, significant wave height values from all seven wave array deployments (30 files) are shown. In Figure 4, wave energy spectral density is plotted for two successive samples within one file.

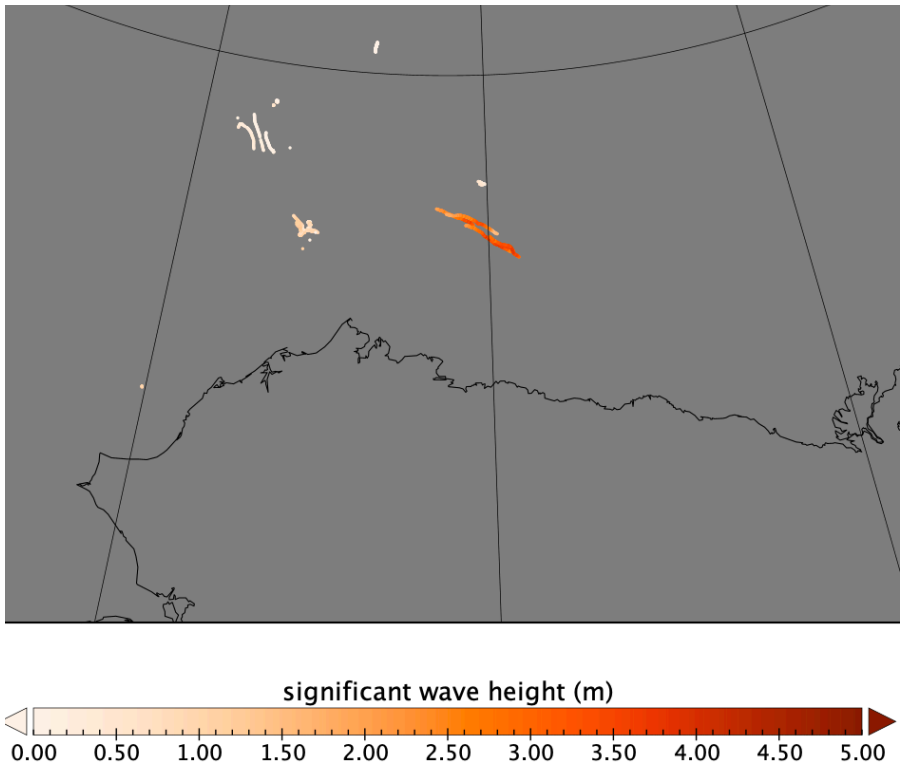

Figure 3. Significant wave height from all the SWIFT NetCDF files plotted using the NASA Panoply NetCDF viewer.

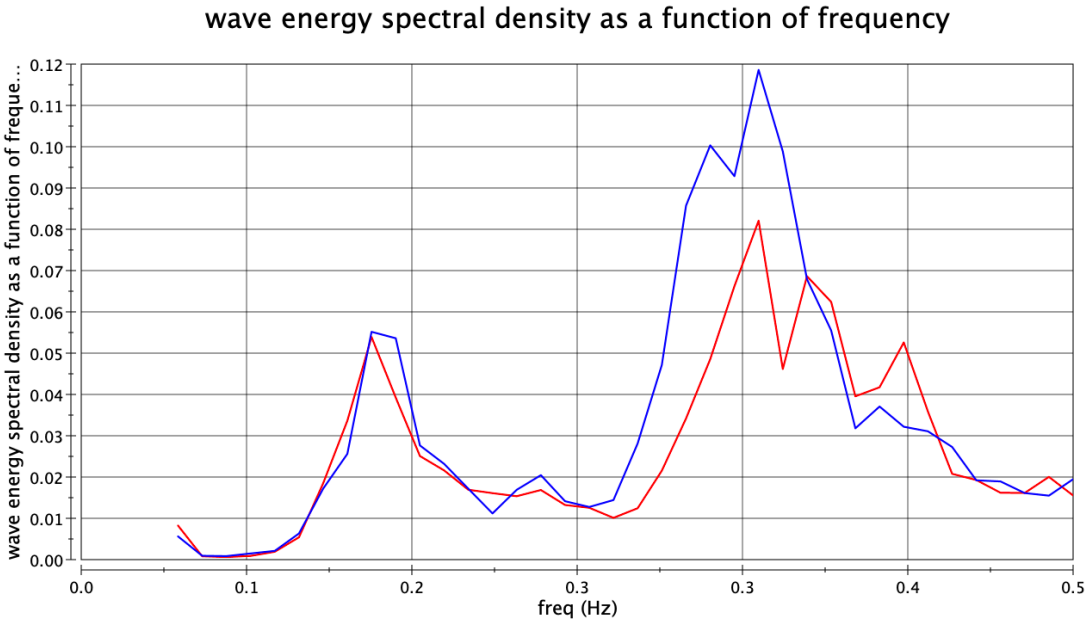

Figure 4. Wave energy spectral density as a function of frequency from 4 October 2015 at 11:44 UTC (red line) and at 12:14 UTC (blue line). These are successive samples from SWIFT14_04Oct2015_30min.nc plotted using the NASA Panoply NetCDF viewer.

2.2 Quality, Errors, and Limitations

Users of the shipboard data will find more information about the quality, potential errors, and limitations of these data in JGR2018.

Notes 1 through 4 in Appendix A are taken from JGR2018 and address some of these issues as they pertain to estimating downwelling radiation measurements, calculating turbulent fluxes, computing significant wave height, and using a surface energy budget technique for estimating ice thickness and concentration.

Users of the SWIFT data will find information on potential uncertainty in SWIFT-data-derived measurements in Smith et al. (2018) and in Thomson (2012).

2.3 Instrumentation

2.3.1 Ship

See JGR2018 for information on instrumentation that acquired the shipboard data. Figure 5 shows where key shipboard instrumentation was located.

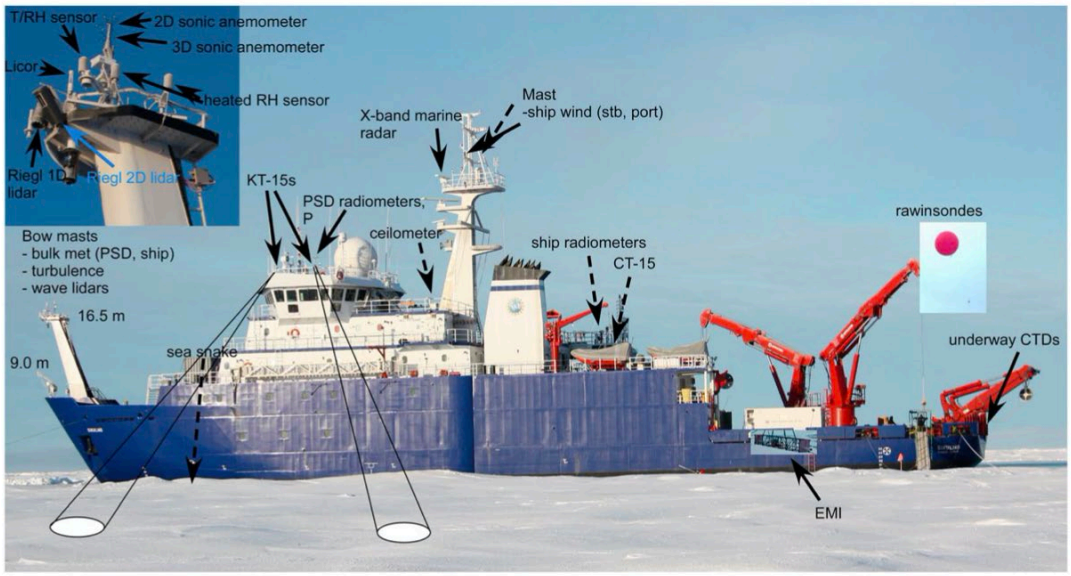

Figure 5. Locations of key meteorological, surface, and upper-ocean instrumentation on the R/V *Sikulaq* during Sea State. Figure from Persson et al. (2018).

2.3.2 SWIFT Drifting Buoy

SWIFT drifters ride the waves and drift with ocean currents (Figure 6). They obtain high-resolution profiles of turbulent velocities collected within 1 m of the surface using a pulse-coherent acoustic

Doppler sonar. Energy dissipation rates due to breaking waves are estimated using turbulent velocity measurements (Thomson, 2012). The drifters measure surface winds, waves, currents, air and water temperature, and salinity as well.

Thomson (2012), Smith et al. (2018), and Smith and Thomson (2019) have more information about the instrumentation on the SWIFT drifters. Figure 6 shows a SWIFT buoy as instrumented in 2012.

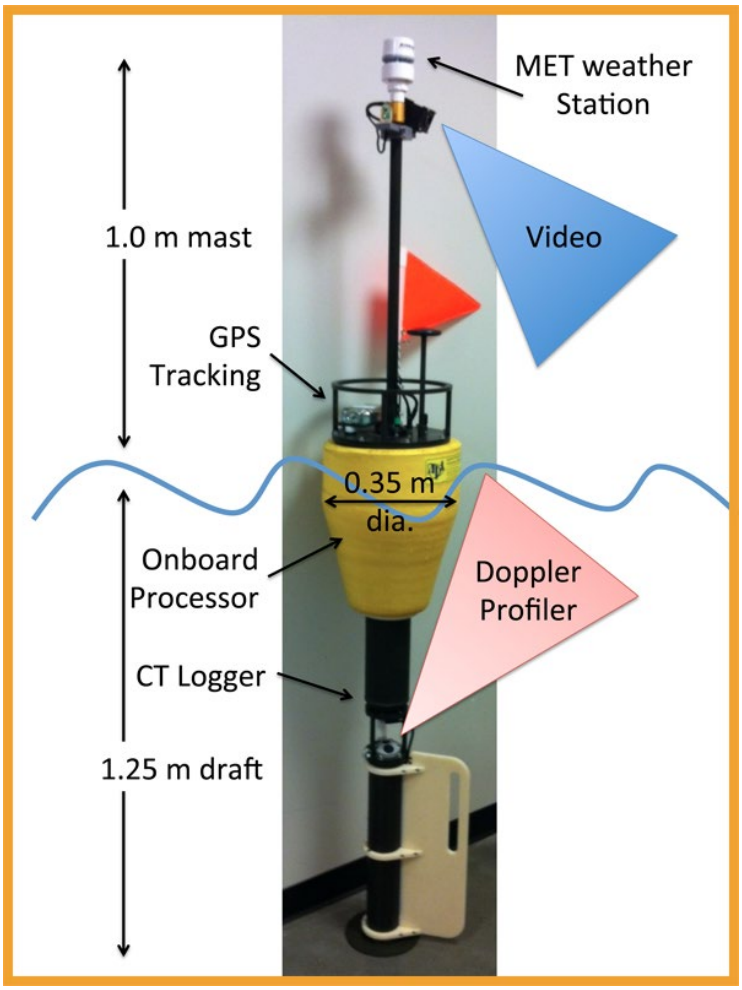

Figure 6. Dimensional drawing of a SWIFT buoy. From www.apl.uw.edu/SWIFT.

3 SOFTWARE AND TOOLS

NetCDF files can be read and used with number of tools, including but not limited to NASA Panoply, Unidata Ncview, PMEL Ncbrowse, Scripps Institution of Oceanography Ncdump, and NetCDF Operators (NCO).

4 VERSION HISTORY

Table 5. Version History Summary

Version	Release Date	Description of Changes	Citation
1	August 2021	Initial Release of these data	Thomson, J. and O. Persson. 2021. *Arctic Sea State 2015 Field Campaign, Version 1*. [Indicate subset used]. Boulder, Colorado USA. NSIDC: National Snow and Ice Data Center. https://doi.org/10.7265/qt2b-y743. [Date Accessed].

5 RELATED DATA SETS

- Long-term measurements of ocean waves and sea ice draft in the central Beaufort Sea

6 RELATED WEBSITES

These data, or portions of these data, may also be available from the sites referenced below.

- The University of Washington Applied Physics Laboratory *Sea State and Boundary Layer Physics of the Emerging Arctic Ocean* website has material compiled when the experiment was being planned and some later information, including lists of investigators, project titles, and publications.
- The University of Washington ResearchWorks Archive served as the first archive for Sea State data. The ResearchWorks Archive collection includes video and other data that we do not archive at NSIDC.
- The Rolling Deck to Repository (R2R) archive for U.S. research vessel data has some of the underway data from the Sikuliaq during Sea State.
- Shipboard ice observations were made following the Arctic Shipborne Sea Ice Standardization Tool (ASSIST) protocol (Hutchings and Faber, 2018). These are archived with the Ice Watch ASSIST Data Network at the Norwegian Meteorological Institute and with PANGAEA (Hutchings, 2018)

7 CONTACTS AND ACKNOWLEDGMENTS

Jim Thomson, Sea State Principal Investigator with the Applied Physics Laboratory at the University of Washington, determined the selection of Sea State data to be archived and published by NSIDC. He reviewed this User Guide prior to its publication online.

Ola Persson, with University of Colorado, CIRES, and the NOAA Physical Sciences Laboratory, provided information about the shipboard data, and reviewed a draft of this User Guide prior to its publication online.

Acknowledged in the cruise report are the Sea State DRI science team, ship's crew, shore team (satellite remote sensing and forecasting), NRL aircraft team, and ONR program managers. Please see ONR Sea State DRI Cruise Report: R/V *Sikuliaq*, Fall 2015 for the names of these people.

These data were prepared for publication and are archived, maintained, and distributed by NSIDC through the support of the Office of Naval Research, Award Number N00014-19-1-2554.

8 REFERENCES

8.1 References specific to Sea State

These references are listed in the order of publication from earlier to more recent. Notes about the research paper, report, or article follow in italics.

Thomson, J. (2012). Wave Breaking Dissipation Observed with SWIFT Drifters. *J. Atmos. Oceanic Technol., 29*(12): 1866–1882. https://doi.org/10.1175/JTECH-D-12-00018.1

Gives an overview of how the rate of energy dissipation through ocean wave breaking can be obtained using data from Surface Wave Instrument Float with Tracking (SWIFT) buoys.

Thomson, J., Squire, V., Ackley, S., Rogers, E., Babanin, A., Guest, P., Maksym, T., Wadhams, P., Stammerjohn, S., Fairall, C., Persson, O., Doble, M., Graber, H., Shen, H., Gemmrich, J., Lehner, S., Holt, B., Williams, T., Meylan, M., and Bidlot, J. (2013). *Science Plan: Sea State and Boundary Layer Physics of the Emerging Arctic Ocean*. Technical Report APL-UW 1306. Applied Physics Laboratory, University of Washington, Seattle.

This Science Plan presents the overall goals and approach of the Sea State field campaign with a focus on the integrated vision of the science.

Harris, M. (2015). Waves of Destruction: Giant Waves Change Arctic Ecology and Weather. *Scientific American*, 312(5), May 2015. https://www.scientificamerican.com/article/giant-waves-change-arctic-ecology-and-weather/.

Sea State was preceded by fieldwork in 2014 that set the stage for the more comprehensive measurement program to follow. This article by M. Harris describes the results of that 2014 field work for a general audience. Big waves were found to have a previously unrecognized role in breaking up ice, thereby contributing to overall ice loss.

Thomson, J. (2015). ONR Sea State DRI Cruise Report: R/V *Sikuliaq*, Fall 2015 (SKQ201512S). 11 November 2015.

The 45-page cruise report is a summary and narrative of the measurements and activities completed during the research cruise, as well as preliminary findings.

Thomson, J., Ackley, S., Shen, H., and Rogers, E. (2017). The balance of ice, waves, and winds in the Arctic autumn, *Eos*, 98. https://doi.org/10.1029/2017EO066029.

Gives an overview of early results, notes the unusual predominance of pancake ice, and describes how the onboard science team operated. Plans were updated daily, with an assist from weather forecasts, wave forecasts, and satellite imagery. The wave model in use at the time performed poorly inside the ice edge and during periods of rapid ice growth or strong wind events. This outcome pointed to areas that later analyses would address.

Guest, P., Persson, O., Wang, S., Jordan, M., Jin, Y., Blomquist, B., and Fairall, C. (2018). Low-level baroclinic jets over the new Arctic Ocean. *Journal of Geophysical Research: Oceans*, *123*(6), 4074-4091. https://doi.org/10.1002/2018JC013778

Soundings described here were used to calculate the mixed-layer height in the shipboard data set time series.

Lund, B., Graber, H. C., Persson, O., Smith, M., Doble, M., Thomson, J., and Wadhams, P. (2018). Arctic sea ice drift measured by shipboard marine radar. *Journal of Geophysical Research: Oceans*, *123*(6), 4298-4321. https://doi.org/10.1029/2018JC013769.

Provides a detailed description of the technique to derive the ocean currents, wave characteristics, and ice drift in the data set from the marine radar data, and their use in the analysis of Sea State conditions.

Persson, O., Blomquist, B., Guest, P., Stammerjohn, S., Fairall, C., Rainville, L., Lund, B., Ackley S., and Thomson, J. (2018). Shipboard observations of the meteorology and near‐surface environment during autumn freezeup in the Beaufort/Chukchi Seas. *Journal of Geophysical Research: Oceans*, 123(7), 4930-4969. https://doi.org/10.1029/2018JC013786.

Describes the collection and processing of shipboard air, ice, and ocean measurements from the Sea State field campaign in the Beaufort/Chukchi Seas in autumn 2015 and the data used to characterize the near-surface freezeup environment.

Persson, O., Blomquist, B., Guest, P., Stammerjohn, S., Fairall, C., Rainville, L., Lund, B., Ackley S., and Thomson, J. (2018). Supporting information for shipboard observations of the meteorology and near-surface environment during autumn freeze-up in the Beaufort/Chukchi Seas. *Journal of Geophysical Research - Oceans, Sea State special issue, 123*. https://doi.org/10.1029/2018JC013786.

The Supporting Information provided in this article includes details of the data processing

for the onboard measured atmospheric and surface parameters from the 2015 Sea State field campaign as well as describing the instrumentation and quality control procedures used. Describes the details of how each parameter was determined.

Smith, M., Stammerjohn, S., Persson, O., Rainville, L., Liu, G., Perrie, W., Robertson, R., Jackson, J., and Thomson, J. (2018). Episodic reversal of autumn ice advance caused by release of ocean heat in the Beaufort Sea. *Journal of Geophysical Research: Oceans*, 123(5), 3164-3185. https://doi.org/10.1002/2018JC013764.

Describes the deployment of eight SWIFT buoys during a storm event over 10-13 October 2015. Uses Sea State SWIFT data and other data to document the melt of sea ice by heat from the upper ocean mixed to the surface during a storm event. Concludes that forcing conditions are related to the changing wave climate in the western Arctic Ocean.

Thomson, J., Ackley, S., Girard‐Ardhuin, F., Ardhuin, F., Babanin, A., Boutin, G., ... & Wadhams, P. (2018). Overview of the arctic sea state and boundary layer physics program. *Journal of Geophysical Research: Oceans*, 123(12), 8674-8687. https://doi.org/10.1002/2018JC013766

Introduces a special section consisting of a series of papers and summarizes the key results of the program that they contain. Users of Sea State data will find context in this overview that will facilitate their work. The overview includes three supplemental videos with supporting information.

Smith, M., and Thomson, J. (2019). Ocean surface turbulence in newly formed marginal ice zones. *Journal of Geophysical Research: Oceans, 124(3)*, 1382–1398. https://doi-org.colorado.idm.oclc.org/10.1029/2018JC014405

Describes results of an analysis of about 350 hours of SWIFT data acquired over 12 buoy deployments between 2 October through 27 October. Uses upper-ocean turbulent dissipation rate profiles from Sea State SWIFT data to explore three turbulence generation regimes: (a) open water; (b) marginal ice zone (MIZ) with energy transfer from wind to ocean occurring via waves; and (c) MIZ with energy transfer from wind to ocean occurring via ice. These three regimes are categorized using the wind, wave, and ice conditions measured during the buoy deployments.

8.2 Other References

Briegleb, B. P., Bitz, C. M., Hunke, E. C., Lipscomb, W. H., Holland, M., Schramm, J. L., & Moritz, R. E. (2004). Scientific Description of the Sea Ice Component in the Community Climate System Model, Version 3 (No. NCAR/TN-463+STR). University Corporation for Atmospheric Research. doi:10.5065/D6HH6H1P.

Fofonff, P., and Millard, R.C. Jr. (1983). Algorithms for computation of fundamental properties of seawater. Unesco Tech. Paper in Marine Science, 44.

Grachev, A. A., Andreas, E. L., Fairall, C. W., Guest, P. S., and Persson, O. (2007). SHEBA flux-profile relationships in the stable atmospheric boundary layer. *Boundary-Layer Meteorology*, *124*(3), 315–333. https://doi.org/10.1007/s10546-007-9177-6.

Groves, J. E., and Stringer, W. J. (1991). The use of AVHRR thermal infrared imagery to determine sea ice thickness within the Chukchi polynya. *Arctic*, *44*, 130–139.

Hutchings, J. K. (2018). Shipborne visual observations of Arctic sea ice. PANGAEA. https://doi.org/10.1594/PANGAEA.889209

Hutchings, J. K., and Faber, M. K. (2018). Sea-Ice Morphology Change in the Canada Basin Summer: 2006–2015 Ship Observations Compared to Observations From the 1960s to the Early 1990s. *Frontiers in Earth Science*, 6, 123.

Lund, B., Zappa, C. J., Graber, H. C., and Cifuentes-Lorenzen, A. (2017). Shipboard wave measurements in the Southern Ocean. *Journal of Atmospheric and Oceanic Technology*, *34*(9), 2113–2126.

Maykut, G. A. (1982). Large-scale heat exchange and ice production in the Central Arctic. *Journal of Geophysical Research*, *87*, 7971–7984.

Persson, O., Fairall, C. W., Andreas, E. L., Guest, P. S., and Perovich, D. K. (2002). Measurements near the atmospheric surface flux group tower at SHEBA: Near-surface conditions and surface energy budget. *Journal of Geophysical Research*, *107*(C10), 8045. https://doi.org/10.1029/2000JC000705.

Spreen, G., Kaleschke, L., and Heygster, G. (2008). Sea ice remote sensing using AMSR-E 89 GHz channels. *Journal of Geophysical Research*, *113*, C02S03. https://doi.org/10.1029/2005JC003384.

Steele, M., Ermold, W., and Zhang, J. (2011). Modeling the formation and fate of the near-surface temperature maximum in the Canadian Basin of the Arctic Ocean. *Journal of Geophysical Research*, *116*(C11015). https://doi.org/10.1029/2010JC006803.

Thomson, J., Talbert, J., de Klerk, A., Brown, A., Schwendeman, M., Goldsmith, J., Thomas, J., Olfe, C., Cameron, G., and Meinig, C. (2015). Biofouling Effects on the Response of a Wave Measurement Buoy in Deep Water. *Journal of Atmospheric and Oceanic Technology, 32*(6). https://doi.org/10.1175/JTECH-D-15-0029.1.

Wang, X., Key, J. R., and Liu, Y. (2010). A thermodynamic model for estimating sea and lake ice thickness with optical satellite data. *Journal of Geophysical Research*, *115*(C12035). https://doi.org/10.1029/2009JC005857.

Wang, X., Key, J., Kwok, R., and Zhang, J. (2016). Comparison of Arctic sea ice thickness from satellites, aircraft, and PIOMAS data. *Remote Sensing*, *8(9)*, 713. https://doi.org/10.3390/rs9090713.

Yu, Y., and Rothrock, D. A. (1996). Thin ice thickness from satellite thermal imagery. *Journal of Geophysical Research*, 101(C10), 25,753–25,766.

9 DOCUMENT INFORMATION

9.1 Author

This document was written by Florence Fetterer in Spring 2021. It was edited and published online by Ann Windnagel.

9.2 Publication Date

August 2021

APPENDIX A – SHIP DATA DETAILED VARIABLE DESCRIPTION

Table A - 1. Detailed description of variables in the ArcticSeaState2015_shipdata.nc file (alphabetical order)

Ref. #	Variable Name	Description	Reference to JGR2018	Data Source	Notes
1	Ai	Best estimate of ice concentration (%)	Sec. 2.4	A mean ice concentration obtained by interpolating the ASSIST hourly estimates to the 10-min time intervals and then averaging the concentrations from the AMSR2, ASSIST, and SEB techniques.	For thin ice, the AMSR2 concentrations are frequently smaller than those from the other techniques, so Ai estimates are often slightly low
2	alb_ref	Surface albedo estimated from the observed surface conditions (ice concentration, snow depth, skin temperature, water freezing point) and subjective estimates of albedo for open water (0.08), thin ice (0.35), thicker ice (0.65) and snow-covered ice (0.85)	Sec. 2.4	Surface albedo is the sum of the albedo of ice times the concentration of ice (Ai) and the albedo of water times the open water area (1-Ai). The albedo of bare ice is assigned based on ice thickness category after Maykut (1982), using the mean of the four ice thickness estimates. The albedo of snow-covered ice is a combination of the albedo of bare ice and that of snow (assumed to be 0.85), weighted by the snow fraction. Snow fraction is determined from the snow depth as in Briegleb et al. (2004). Snow depth is from the ASSIST observations.	
3	cld_bas_ref	Median cloud base from ceilometer (m)	Sec. 2.1, Table 1	Ceilometer measurements every 15 s, averaged to 10 min	Vaisala CT25K ceilometer
4	cld_frc_ref	Cloud fraction (%); percent of time within 10-min period that ceilometer detected a cloud	Sec. 2.1, Table 1	Ceilometer measurements	Vaisala CT25K ceilometer
5	cog_ref	Course over ground (degrees) from GPS		Ship navigation data	Also see #12, hed_ref

Ref. #	Variable Name	Description	Reference to JGR2018	Data Source	Notes
6	ctd6m_frzT_ref	Freezing point at 6 m depth (deg C)		Calculated using T and S from the profiling CTD and using Fofonff and Millard (1983)	
7	ctd6m_S_ref	CTD salinity at 6 m depth (psu)	Table 3, "S"	The measurement at 6m from an underway profiler.	Teledyne Ocean Science underway CTD 16 Hz, ~11 min, 4 m–150 m depth
8	ctd6m_T_ref	CTD temperature at 6 m depth (deg C)	Table 3, "To"	The measurement at 6m from an underway profiler.	Teledyne Ocean Science CTD 16 Hz, ~11 min, 4 m–150 m depth
9	emiss_ref	Surface emissivity estimated from surface type/conditions: 0.990 (open water) or 0.985 (ice covered water)	Sec. 2.4	Longwave surface emissivity is the sum of the emissivity of ice times the concentration of ice (Ai) and the emissivity of water times the open water area (1-Ai).	
10	fatm	Net atmospheric energy flux fatm=swd_bst_ref – swu + lwd_bst_ref – lwu - hs_blk_ref - hl_blk_ref (W/m^2)	Table 4, "fatm"	Calculated from observed and derived values for downwelling shortwave radiation, upwelling shortwave radiation, downwelling longwave radiation, upwelling longwave radiation, sensible heat flux, and latent heat flux.	fatm is the total heat exchange between the surface and the atmosphere. See Note (1) on riming.
11	floe_size_ref	ASSIST floe size code for ice type with greatest concentration: 100 for pancakes; 200 for new sheet ice; 300 for brash/broken ice; 400 for cake ice, <20m; 500 for small floes, 20-100m; 600 for medium floes, 100-500 m; 700 for large floes, 500-2000 m; 800 for vast floes, >2000m; 900 for bergy floes	Sec. 2.2, Table 2	Hourly visual observations from the ship's bridge for estimates of floe sizes following the ASSIST protocol.	The area viewed by the observers was limited to the nearest ~2-km range during daylight hours and to the ship vicinity illuminated by a floodlight during night. Observers were trained prior to the cruise.
12	hed_ref	GPS heading (degrees)		Ship navigation data are averaged over 10 minutes.	Also see #5, cog_ref
13	hl_blkr	latent heat flux -bulk as for sensible heat flux (W/m^2)	JGR2018 Sec. 2.4	See Note (2) on bulk turbulent fluxes	
14	hlc_ref	latent heat flux - covariance (W/m^2)	JGR2018 Sec. 2.4	See Note (2) on bulk turbulent fluxes	

Ref. #	Variable Name	Description	Reference to JGR2018	Data Source	Notes
15	hlid_ref	latent heat flux - inertial dissipation (W/m^2)	JGR2018 Sec. 2.4	See Note (2) on bulk turbulent fluxes	
16	hs_blkr	sensible heat flux - bulk calculated using COARE and SHEBA flux (W/m^2) schemes depending on mosaic method & mean ice concentration. Neither scheme was developed for mixed waves and ice.	JGR2018 Sec. 2.4	See Note (2) on bulk turbulent fluxes	
17	hsc_ref	sensible heat flux -covariance (W/m^2)	JGR2018 Sec. 2.4		
18	hsid_ref	sensible heat flux - inertial dissipation (W/m^2)	JGR2018 Sec. 2.4		
19	Hsig_Rgl_ref	significant wave height from 1-D Riegl (m)	Sec. 2.2, Table 2	The 1-D Riegl lidar provided a distance to the ocean surface, which was combined with ship-motion measurements to obtain wave heights at 10 Hz temporal resolution.	See Note (3)
20	ice_concvo_ref	total ice concentration from visual observations, 0-10 (tenths)	Sec. 2.2, “ICA”	Hourly visual observations from the ship’s bridge for estimates of total ice concentration following the ASSIST protocol.	The area viewed by the observers was limited to the nearest ~2-km range during daylight hours and to the ship vicinity illuminated by a floodlight during night. Observers were trained prior to the cruise.
21	ice_typ1vo_ref	primary ice type from visual observations	Sec. 2.2	Hourly visual observations from the ship’s bridge for Ice type following the ASSIST protocol.	The area viewed by the observers was limited to the nearest ~2-km range during daylight hours and to the ship vicinity illuminated by a floodlight during night. Observers were trained prior to the cruise.

Ref. #	Variable Name	Description	Reference to JGR2018	Data Source	Notes
22	ice_z_ref	ice thickness estimates from visual observations (cm)	Sec. 2.2, “tkA”	Hourly visual observations from the ship’s bridge for Ice thickness following the ASSIST protocol.	The area viewed by the observers was limited to the nearest ~2-km range during daylight hours and to the ship vicinity illuminated by a floodlight during night. Observers were trained prior to the cruise.
23	iceconcSEB_ref	10-min ice concentration from surface energy budget thermodynamic technique (%)	Sec. 2.4, “ICT”	10-minute average ice thicknesses are calculated from surface temperatures measured by the KT-15 IR thermometers. The measured skin temperature, wind, ocean freezing point, and energy fluxes are combined with surface energy budget equations to estimate ice thickness over ~3-m wide spots	See Note (4) on surface energy budget technique for ice thickness and concentration
24	iconcsh_amsr_ref	ice concentration from daily AMSR2 (3.125 km res) (%)	Sec. 2.4, Table 4	AMSR2 (Spreen et al., 2008)	Spurious ice concentrations over open water, which can result from weather effects on the AMSR2 retrievals were not noted along the ship track.
25	ieaz_ref	azimuth to nearest ice edge (degrees)	Sec. 2.4	Direction to the nearest ice edge is derived from the ship’s location and the AMSR2 ice concentration field, at points at which ice drift speed and direction are determined using the marine radar.	The ice edge is defined as the location of an ice concentration less than 15%.

Ref. #	Variable Name	Description	Reference to JGR2018	Data Source	Notes
26	iedis_ref	distance to nearest ice edge (km)	Sec. 2.4	Distance to the nearest ice edge is derived from the ship's location and the AMSR2 ice concentration field, at points at which ice drift speed and direction are determined using the marine radar.	The ice edge is defined as the location of an ice concentration less than 15%.
27	ieor_ref	orientation of nearest ice edge (degrees)	Sec. 2.4	Ice edge orientation is derived from the ship's location and the AMSR2 ice concentration field, at points at which ice drift speed and direction are determined using the marine radar.	The ice edge is defined as the location of an ice concentration less than 15%.
28	jd_ref	decimal day-of-year at start of averaging interval		Time (as decimal day of year) at start of 10-minute interval. Day of year is in 2015.	
29	lat_ref	Latitude (degrees)		From ship navigation data.	Also see #12, hed_ref Also see #5, cog_ref
30	lon_ref	Longitude (+/- 180 deg)		From ship navigation data.	Also see #12, hed_ref Also see #5, cog_ref
31	lwd_bst_ref	downwelling LW radiation, gaps estimated from ceilometer & soundings (W/m^2)	Sec. 2.1 Note 5	Measured from two Eppley Precision Solar Pyranometers (PSPs) and two Eppley Precision Infrared Radiometers	See Note (1) on riming
32	lwd_med_ref	downwelling LW radiation, manually edited (W/m^2)	Sec. 2.1 Note 5	Measured from two Eppley Precision Solar Pyranometers (PSPs) and two Eppley Precision Infrared Radiometers	See Note (1) on riming
33	lwu	upwelling longwave radiation estimated from composite skin temperature, estimated surface emissivity, and Stefan-Boltzmann relation & mosaic method with ice concentration (W/m^2)		"mosaic method" arrives at an estimate weighting by fractional proportion of surface type.	

Ref. #	Variable Name	Description	Reference to JGR2018	Data Source	Notes
34	mlh_ref	atmospheric mixed-layer height at times of soundings (m)	Sec. 2.4, Table 4	Rawinsonde soundings were made regularly [4 times a day-?] The atmospheric mixed-layer height (AMLH) for each sounding was calculated as the lowest height at which the vertical gradient in virtual potential temperature (θv) becomes greater than 1°C/110 m over a layer at least 100-m thick.	To avoid artificial inversions caused by the ship's heat island or stack plume, the processing algorithm only considers heights of 100 m or more.
35	omld_ref	Ocean mixed-layer depth from uCTDs (m)	Sec 2.5, "AMLH", Table 4	The ocean mixed-layer depth for each underway CTD profile was computed by finding the top depth that had a potential density that was at least 0.2 kg/m3 greater than the mean density in the top 10 m (e.g., Steele et al., 2011)	
36	omlheat_ref	heat content of ocean mixed layer (J/m^2)	Sec 2.5, Table 4	From underway CTD data	
37	omlp15heat_ref	heat content of ocean mixed layer between OML and OML+15 m (J/m^2)	Sec 2.5, Table 4		
38	omlxcsheat_ref	excess heat content (above freezing point) of ocean mixed-layer (J/m^2)	Sec 2.5, Table 4	Ocean freezing point (Tfrz) and ocean excess temperature (Toxcs = To - Tfrz) are calculated from salinity by standard relationships (Fofonff & Millard, 1983).	
39	p_mb_ref	atmospheric pressure at height zp (mb)	JGR2018 Supplement Note 1	The mean of two sensors	Also see #77, #54
40	pcp_ref	precipitation rate (set to 0.1 mm/h when logs indicated precipitation; otherwise 0)			
41	qa_ref	specific humidity (g/kg)			Also see #78
42	qs_ref	surface saturation specific humidity (g/kg)			
43	radar_icedrift_dir_ref	Marine radar ice drift direction (degrees clockwise from N)	Sec. 2.4, Table 4	From marine radar backscatter fields (Lund et al., 2017)	Acquired every 30 minutes

Ref. #	Variable Name	Description	Reference to JGR2018	Data Source	Notes
44	radar_icedrift_spd_ref	marine radar ice drift speed (m/s)	Sec. 2.4, Table 4	From marine radar backscatter fields (Lund et al., 2017)	Acquired every 30 minutes
45	radar_sfccurr_dir_ref	marine radar surface current direction (degrees clockwise from N)	Sec. 2.5, Table 2	From resolved waves in marine radar backscatter fields (Lund et al., 2017)	
46	radar_sfccurr_spd_ref	marine radar surface current speed (m/s) (B. Lund)	Sec. 2.5, Table 2	From resolved waves in marine radar backscatter fields (Lund et al., 2017)	
47	radar_wave_dp_ref	marine radar peak wave direction (degrees clockwise from N)	Sec. 2.5, Table 2	From resolved waves in marine radar backscatter fields (Lund et al., 2017)	
48	radar_wave_tp_ref	marine radar peak wave period (s)	Sec. 2.5, Table 2	From resolved waves in marine radar backscatter fields (Lund et al., 2017)	
49	rh_ref	relative humidity (%)	Sec. 2.1, Table 1; Supplement Note 3		Referred to as RHa, measured by the Vaisala instrument
50	rwdir_ref	relative wind dir, composite (+/- 180 deg from bow)	Sec. 2.1, Table 1	The PSD anemometer is used unless the ship relative wind direction exceeds +-120 deg. In that case the main mast anemometer for the windward side is used.	
51	rwspd_ref	relative wind speed, composite (m/s)	Sec. 2.1, Table 1	The PSD anemometer is used unless the ship relative wind direction exceeds +-120 deg. In that case the main mast anemometer for the windward side is used.	
52	sal_ref	salinity at ship intake at 6.5 m depth (PSU)			

Ref. #	Variable Name	Description	Reference to JGR2018	Data Source	Notes
53	slp_ref	sea-level pressure by height-correcting p_mb_ref (mb)	Sec 2.1: 1	The air pressure at 17 m is the mean value of the PSD PTB220 and the ship PTU307 sensors. It is then height adjusted to produce the mean sea level pressure (MSLP).	
54	snow_z_ref	snow depth estimates from visual observations (cm)	Sec 2.2, Table 2	Hourly visual observations from the ship's bridge for snow depth following the ASSIST protocol.	Every 60 minutes to the nearest 10-minute interval.
55	sog_ref	gps speed over ground (m/s)			
56	std_hed_ref	std deviation in gyro heading (degrees)			
57	std_rwdir_ref	std deviation relative wind direction, composite (degrees)			
58	std_rwspd_ref	std deviation relative wind speed, composite (m/s)			
59	std_sog_ref	std deviation in speed over ground (m/s)			
60	swd_bst_ref	downwelling SW radiation, manually edited, linear interpolation across gaps (W/m^2)	S1, text and figure	Measured from two Eppley Precision Solar Pyranometers (PSPs) and two Eppley Precision Infrared Radiometers and manually edited. This gap-filled variable is considered "best".	See Note (1) on riming
61	swd_med_ref	Downwelling SW radiation, manually edited (W/m^2)	S1, text and figure	Measured from two Eppley Precision Solar Pyranometers (PSPs) and two Eppley Precision Infrared Radiometers and manually edited. "Here we use the median values of the manually edited, 10-min mean, downwelling radiation from each of the two pairs of PSD radiometers, with or without the missing data filled in through linear interpolation between good data points. The former is considered the "best" data set. "	See Note (1) on riming

Ref. #	Variable Name	Description	Reference to JGR2018	Data Source	Notes
62	swu	Upwelling shortwave radiation estimated from best downwelling SW radiation and estimated surface albedo & mosaic method with ice concentration (W/m^2)			See Note (1) on riming
63	ta_ref	air temperature (degrees C)		Air temperatures (Ta) from the HMT337 are used, but values from any of the other sensors, which all agree within 0.2°C, are used if HMT337 data are missing (very rare).	
64	tau_blkr	bulk stress (N/m^2), as for sensible heat flux			
65	tauc_ref	stress - covariance (N/m^2)			
66	tauid_ref	stress - inertial dissipation (N/m^2)			
67	to_frz_ref	freezing point of sea water from salinity from ship intake at 6.5 m depth (degrees C)		From ship water intake salinity and using Fofonff and Millard (1983)	
68	Tpi_Rgl_ref	max wave period from 1-D Riegl (s), Doppler corrected ala (Collins et al. 2017)			
69	ts_skn_ref	composite skin temperature from ship-based IR sources (degrees C)			
70	ts_snk_ref	sea-snake temperature when deployed at either 10 cm depth or on top of ice/snow (degrees C)			
71	wdir_ref	true wind direction, composite (degrees)			
72	wspd_ref	true windspeed, composite (m/s)			
73	zice_dpnt_ref	ice thickness from dipnet (P. Wadhams) (m)			
74	ziceSEBmd_ref	10-min median of 1-s ice thickness from thermodynamic technique (m), mean of two KT-15 radiometers			
75	zicesig_ref	10-min standard deviation of 1-s ice thickness values from thermodynamic technique (m)			

Ref. #	Variable Name	Description	Reference to JGR2018	Data Source	Notes
76	zp_ref	air pressure measurement height (m)		The air pressure at 17 m is the mean value of the PSD PTB220 and the ship PTU307 sensors. It is then height adjusted to produce the mean sea level pressure (MSLP).	
77	zq_ref	air humidity measurement height (m)			
78	zt_ref	air temperature measurement height (m)			
79	zu_ref	wind speed measurement height, composite (m)			

Note (1) on riming, from JGR2018:

Instrument riming was the major problem for accurate downwelling radiation measurements during Sea State, as Ta was below freezing, the RH was high, supercooled fog drops were frequently observed, and even sea spray occurred on a few occasions with strong winds over open water. Riming can produce up to a ~40–80 W/m2 positive error for a given LWd value, but it is nearly impossible to discern whether riming is occurring from the LWd measurement itself."

The six radiometers on the R/V Sikuliaq were manually cleaned several times per day, and a careful log was kept of the degree of riming during each visit. This information was used to edit and correct the downwelling radiation data as described in the supporting information Text S1. Linear interpolation was done between remaining good data.

Downwelling shortwave radiation (SWd) was also manually edited based on the observed degree of riming at the time of cleaning, and linear interpolation was also done between the remaining good values. Zero values were inserted whenever the solar zenith angle was greater than 90°. The impact of editing on SWd was significantly smaller than for LWd because clear-sky midday values of SWd were < 150 W/m^2 for the campaign and frequently <50 W/m^2. For both LWd and SWd, we use the median values of the manually edited, 10-min mean, downwelling radiation from each of the two pairs of PSD radiometers, with or without the missing data filled in through linear interpolation between good data points. The former is considered the best data set.

Note (2) on bulk fluxes, from JGR2018:

Bulk turbulent fluxes are calculated separately over the ice and water portions of the scene, using the same atmospheric values for each. Over ice, the scheme used is the one from Persson et al. (2002) based on SHEBA measurements, but with the stability correction functions of Grachev et al. (2007). Over water, the COARE3.0 scheme (Fairall et al., 2003) is used but only with the Charnock and viscosity estimates of surface roughness and not the wave parameters. The net turbulent flux is then calculated by weighting each appropriately with the ice fraction, as given by:

$$H_s = A_i H_{si} + (1 - A_i) H_{sw}$$

$$H_l = A_i H_{li} + (1 - A_i) H_{lw}$$

$$\tau = A_i \tau_i + (1 - A_i) \tau_w$$

where H_s and H_l are the sensible and latent heat fluxes, respectively, τ is the stress, and X_i and X_w are the turbulent fluxes of X from the SHEBA and COARE schemes, respectively. This approach to bulk turbulence estimation is only marginally satisfactory, as neither the SHEBA scheme, developed for thick multiyear ice, nor the COARE scheme, developed for open-ocean conditions, are appropriate for this environment. Specifically, the surface roughness in this marginal ice zone environment is likely different than those for which these two schemes were developed. However, comparisons between this combination of the two bulk schemes with 10-min direct covariance fluxes shows reasonable agreement in the mean (see sections 4 and 5), though with significant scatter. Schemes such as that by Andreas et al. (2010), which uses an ice fraction- dependent roughness length or that of Lüpkes et al. (2012), which considers ice fraction, freeboard, and floe sizes, are likely more appropriate and are currently being tested. The reason they are not directly used here is because they were developed for thicker ice (greater freeboard) than is observed with this thin, growing ice during Sea State.

Note (3) on significant wave height, from JGR2018:

10-min significant wave heights are computed as 4 times the square root of the zeroth moment of the motion-corrected wave height spectra (moment technique) and as 4 times the standard deviation of the measured surface height displacements (CF method).

The first method is more accurate but requires that at least 50% of the samples during the 10-min time period are available, while the latter can obtain reasonable values with more missing data. Low infrared reflectivity of smooth water and ice surfaces and possibly icing on the lidar optics were the major reasons for missing data.

Note (4) on surface energy budget technique for ice thickness and concentration, from JGR2018:

The ship-based, surface energy budget (SEB) technique used here improves on related satellite-based algorithms used by Groves and Stringer (1991), Yu and Rothrock (1996), and Wang et al. (2010, 2016) and provides raw thickness estimates at 1-Hz temporal resolution (the temporal resolution of the KT- 15 instruments). Hence, it also allows an estimate of ice concentration for each 10-min period nominally along a 1.8-km track, assuming a ship speed of 3 m/s.